GOSPODARKA SUROWCAMI MINERALNYMI – MINERAL RESOURCES MANAGEMENT
2020 Volume 36 Issue 1 Pages 37–58
DOI: 10.24425/gsm.2020.132549

KAROL ZGLINICKI[1], KRZYSZTOF SZAMAŁEK[2], GUSTAW KONOPKA[3]

Monazite-bearing post processing wastes and their potential economic significance

Introduction

Rare earth elements (REE) are essential mineral raw material for highly developed economies (Goodenough et al. 2018; Zhou et al. 2017). It is estimated that the global REO demand for clean technologies by 2030 will reach the level of 50 kt REO (Zhou et al. 2017). As a consequence of the limited Chinese supply of REE and high metal prices, new exploration and production projects will have to be developed in previously poorly recognized regions and sea bottom sediments (Yasukawa et al. 2015). The increase of global demand for REE and the unstable situation on the raw material markets make it necessary to search for new, alternative sources (European Commission 2017). Fluctuations in REE prices on the world markets and high demand make it necessary to revise the previously identified and until now undeveloped primary and secondary placer deposits of sands enriched with REE carriers. Products of processing: red muds with bauxite processing (Deady et al. 2014), coal ash

✉ Corresponding Author: Krzysztof Szamałek; e-mail: krzysztof.szamalek@pgi.gov.pl
[1] Polish Geological Institute, Warszawa, Poland; ORCID iD: 0000-0001-8463-3929; e-mail: karol.zglinicki@pgi.gov.pl
[2] Polish Geological Institute, Warszawa, Poland; ORCID iD: 0000-0002-7487-5243; e-mail: krzysztof.szamalek@uw.edu.pl
[3] Institute of Ceramic and Building Materials, Warszawa, Poland; e-mail: gustaw.konopka@gmail.com

(Periravi et al. 2017), tailings after processing of cassiterite bearing sands (Szamałek et al. 2013) and collected by urban mining – batteries, permanent magnets as well as spent mobile phones (Szamałek and Galos 2016), may be sources to increase the supply of raw materials of strategic importance.

Monazite, among 250 known minerals containing REE, is one of the most important minerals as the primary source of REE (Kanazawa and Kamitani 2006; Simandl 2014; Golev et al. 2014). The largest placer deposits of monazite have been found on the coasts of India, Australia, Malaysia and Indonesia (Haldar 2013; Hoatson et al. 2011; Szamałek et al. 2013).

In 2013, a team of Polish geologists examined the potential deposits of the Indonesian island of Bangka (Szamałek et al. 2013). During the field works, samples of mineral wastes resulting from the processing of alluvial and marine cassiterite placer deposits were collected. The dominant tailing mineral was found to be monazite. The chemical composition of the tailing was examined and the presence of radioactive intergrowth was identified. The percentage of monazite content in the waste after the processing of cassiterite bearing sediments was estimated. Tailing enriched with monazite from the Bangka Island may be a new potential source of REE.

1. Geological setting

Bangka Island (Fig. 1) is the final, southern part of the Tin Belt of Southeast Asia stretching from Burma and Thailand through the Malay Peninsula to Indonesian islands (Schwartz and Surjono 1991; Schwartz et al. 1995). The tectonic history of the area is connected with the processes of subduction and accretion of terranes, arches of Sibumasu islands (acronym China-Siam-Burma-Malaysia-Sumatra) from the Indochina terrane during the closure of the Paleo-Tethys from Devonian to Middle Triassic and Neo-Tethys from the Permian to the Paleogene (Metcalfe 2002; Searle et al. 2012). The effect of the tectonic evolution was the creation of three granite provinces with different geochemical and petrological indexes (Schwartz et al. 1995; Hutchison and Taylor 1978):

1) the Western Granite Province with Cretaceous granites (type S and I);
2) the Eastern Granite Province with Permian-Triassic granites (type I);
3) the Central Granite Province with dominance of Triassic granites (type S).

Indonesian granites are the southern continuation of the Main Range granite provinces (Wai-Pan Ng et al. 2017).

On Bangka Island, 4 stratigraphic sedimentary sequences, as well as 2 main and 13 smaller magma batholiths were recognized (Ko Ko 1986). The sedimentary series (basement) includes formations from the Upper Paleozoic to the Upper Triassic of the Pemali Group and Tempilang Sandstone (Ko Ko 1986; Schwartz and Surjono 1991; Schwartz et al. 1995). The Paleogene-Quaternary series are formed by poorly exposed sediments of Fan Formation and Ranggam Group (Ko Ko 1986). At the turn of the Permian and Triassic

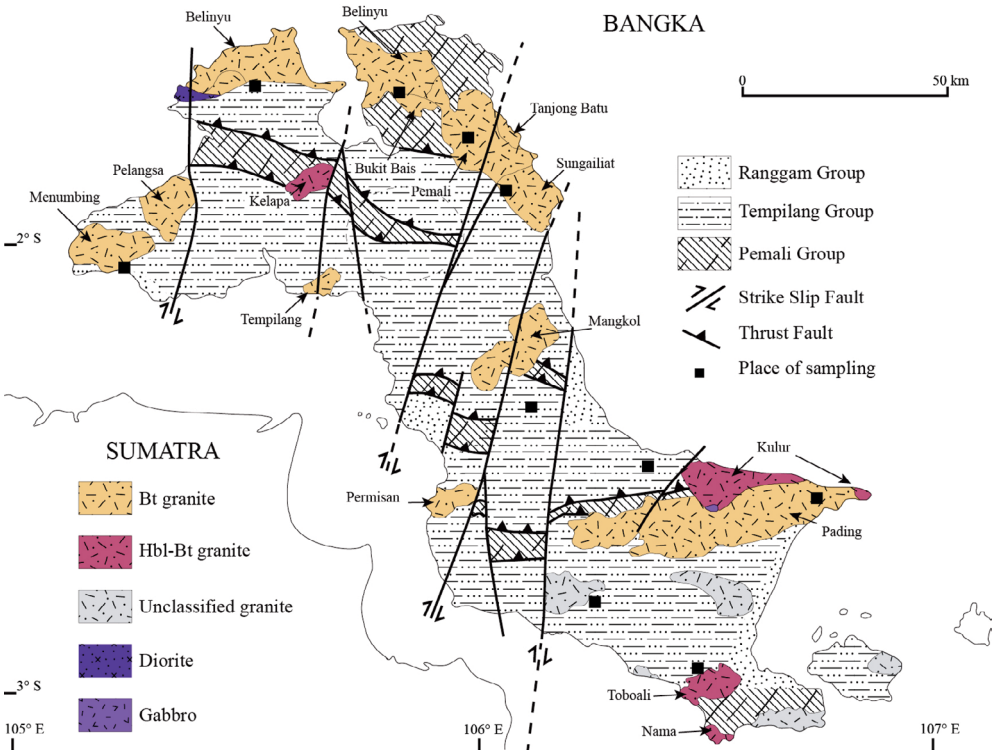

Fig. 1. Geological map of Bangka Island after
Ko Ko 1986; Cobbing et al. 1992; Schwartz et al. 1995; Wai-Pan Ng et al. 2017

Rys. 1. Mapa geologiczna Wyspy Bangka

periods, the sedimentary sequence was intruded by magma rocks of broad composition from gabbro to granite (Aleva 1960; Priem et al. 1975; Ko Ko 1986; Schwartz and Surjono 1991). Granite plutons are characterized by variability of types and sorts of magma rocks – granites I or S-types (Wikarno et al. 1984). Biotite granite, hornblende – biotic granite, two – mica granite, pegmatite granite, pegmatite and aplite in the form of a lens are present in the granite structures (Schwartz and Surjono 1991; Schwartz et al. 1995). Rocks usually contain mega crystals of: potassium feldspar, plagioclases, quartz, biotite, hornblende and muscovite. Accessory minerals include: apatite, titanite, allanite, topaz, monazite, xenotime, zircon (Wikarno et al. 1984; Wai-Pan Ng et al. 2017; Schwartz et al. 1995). The main opaque oxide of Fe is ilmenite, while galena, chalcopyrite and pyrite are secondary.

Granites from Bangka Island are classified as ilmenite-series granites (Ishihara 1977). The manifestations of granite magmatism were closely connected with hydrothermal and metasomatic processes, which led to the formation of rich, primary tin mineralization (Schwartz and Surjono 1991) associated with greisens, granites and pegmatites. Minerals

occurring in veins are: quartz, cassiterite, magnetite, tourmaline, pyrite, marcasite, pyrrhotite, arsenopyrite, chalcopyrite, galena, tennantite, rutile, wolframite and others (Schwartz et al. 1995).

The presence of xenotime and monazite is associated with hydrothermal veins. Granite rocks underwent intensive chemical weathering processes under tropical conditions lasting from the Neogene to the present day. The product of the weathering was the formation of kaolin covers *in situ*, alluvial placer deposits, and off-shore and on-shore deposits being the extension of flooded paleo-valleys (Schwartz et al. 1995).

2. Materials and methods

2.1. Materials

During the prospecting season on Bangka Island, 35 samples of tailings (formed during the processing of cassiterite bearing sands) were collected. The detailed characteristic of the processing technology of the cassiterite bearing sediments is described by Szamałek (Szamałek et al. 2013). The tailings were formed in a 3-stage tailing process and are characterized by an exceptional mineralogical richness (Szamałek et al. 2013). Study material was collected from the landfills (Figs. 2A,B) mined by 10 local artisanal mineral processors – compradors. Tailing is stored in numerous jute bags and therefrom the samples were collected (top, middle, bottom of the jute bag). Thereafter, collected samples were averaged, using a manual PCV sampler 30 cm long and 5 cm wide. The weight of the samples was about 500 g. Loose sediment was prepared for the study, reduced to 50 g by quartering method. Microscopic preparations (slides) were made from samples of tailing. The location

Fig. 2. (A) Bags with tailing from artisanal mining. (B) Tailing dump of state owned mining companies

Rys. 2. (A) Torby zawierające odpady przeróbcze z rzemieślniczych kopalni.
(B) Miejsce składowania odpadów przeróbczych z państwowych kopalni

of samples collecting is presented on the geological map (Fig. 1). Artisanal processing plants are located at the distance of up to 15 km from small mines operated in neighboring granite massifs.

2.2. Methods

A mineral composition analysis was performed with AXS D8 Bruker Davinci diffractometer equipped with a Lynx Eye PSD detector, automated optics, Cu lamp, and Ni Kb filter. Settings included 5-100 2Θ range, primary slit 0.30, secondary slit 1.50, soller slits 2.50, counting time 2s/step, and step size 0.010 2Θ. Identification of the mineral phases was carried out using Bruker Evaluation v.2 software with ICDD PDF-2 v. 2007 and

Table 1. Conditions EPM analyses for monazite grains

Tabela 1. Warunki analizy EPM monacytu

Element	Standard	Analytical line	Crystal	Detection limit in σ (wt.%)	σ (wt.%)
Si	Wollastonite	Kα	TAP	0.01	0.01–0.03
P	Apatite	Kα	LPET	0.02	0.20–0221
Ca	Wollastonite	Kα	LPET	0.01	0.01
La	$LaPO_4$	Lα	LLIF	0.11–0.12	0.40–0.56
Ce	$CePO_4$	Lα	LLIF	0.12–0.13	0.53–0.64
Pr	$PrPO_4$	Lβ	LLIF	0.14–0.15	0.21–0.23
Nd	$NdPO_4$	Lβ	LLIF	0.06	0.05
Sm	$SmPO_4$	Lα	LLIF	0.07	0.07
Eu	$EuPO_4$	Lα	LLIF	0.03–0.06	0.03
Gd	$GdPO_4$	Lα	LLIF	0.03	0.04–0.07
Tb	Tb glass	Lα	LLIF	0.04	0.04
Dy	$DyPO_4$	Lα	LLIF	0.04–0.05	0.08–0.11
Ho	$HoPO_4$	Lβ	LLIF	0.1	0.09
Er	$ErPO_4$	Lα	LLIF	0.04–0.05	0.07–0.09
Tm	Tm glass	Lβ	LLIF	0.05	0.05
Yb	$YbPO_4$	Lα	LLIF	0.06	0.07–0.09
Lu	Lu glass	Lβ	LLIF	0.12	0.11
Y	Y glass	Lα	LPET	0.03	0.04–0.05
Th	Th glass	Mα	LPET	0.04	0.04–0.07
U	U glass	Mβ	LPET	0.04–0.06	0.05–0.07

PDF 4+ v. 2011 databases. The mineralogical analysis was conducted using the Retvield method implemented in Bruker Topas v. 4.2 software. The research was carried out at the Institute of Ceramics and Building Materials in Warsaw.

The observations of tailing were carried out using a scanning microscope ΣIGMA VP with two EDS (SDD XFlash | 10) detectors from Bruker. The analyses were performed at an accelerating voltage of 25 kV in a high vacuum. The analysis of the chemical composition of monazites in the micro-area was performed using the CAMECA SXFiveFe electron microprobe equipped with wave dispersion spectrometers (WDS). The studies were conducted at the Inter-Institute Analytical Complex for Minerals and Synthetic Substances of the University of Warsaw. Thin sections for micro-area investigations were coated with carbon. The analyses were performed at accelerating voltage 15 kV, beam current 20 nA, beam diameter around 1 μm, peak count time 20 s, and background time 10 s. The spectra were analyzed on individual spectrometers equipped with crystals (TAP, LLIF, LPET). The limits of detection, standards used and standard deviation (wt.%) are presented in Table 1.

The gamma-ray spectrum of the sample was measured with a 5 cm diameter and 7 cm high HPGe germanium detector. The detector was placed in a lead “house” with a wall thickness of 10 cm, with an additional inner layer of copper to prevent the formation of X-rays in the lead due to interaction with β particles emitted from the sample.

The energy and performance calibration of the detector was performed with a ^{152}Eu calibration source with an intensity placed at a distance of 1 cm from the detector. Fourteen lines with energies from 121 to 1408 keV were selected for calibration. A FWHM resolution of 0.15% was obtained for 1408 keV line,. The energy calibration allowed to determine the energy of the line with the accuracy of 0.2 keV. Then, for 73060 seconds, the background of an empty house was measured. Due to the fact that the sample contains the same isotopes as the natural background, it is necessary to measure them without the presence of the sample. The sample was then placed in the same place as the calibration source and its radiation was measured for a period of 51135 s.

3. Results and discussion

3.1. Mineralogy of tailing

An analysis of mineral composition (Figs 3–4) indicates that tailing is of a polymineral nature. The tailing is composed of numerous minerals: quartz, plagioclases, pyrite, marcasite, tourmaline and minerals of deposit importance: monazite, xenotime, zircon, malayaite, cassiterite, anatase, struverite, aeschynite-(Y) and ilmenite, rutile, pseudo rutile. Depending on the applied processing technology of cassiterite bearing sands and their region of origin, the obtained percentage of industrial minerals may vary (Table 2).

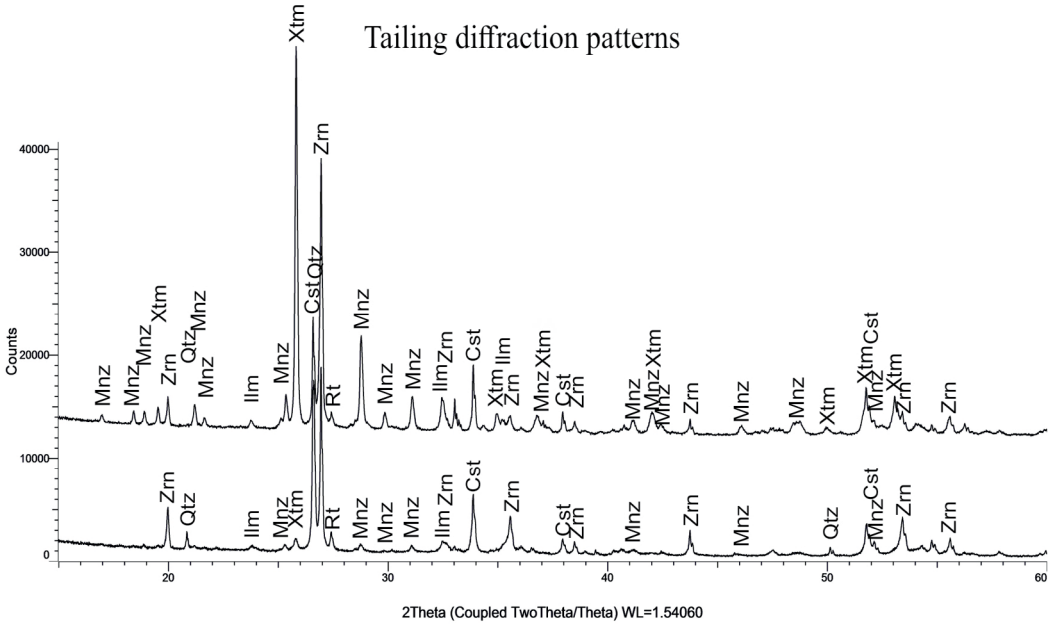

Fig. 3. Diffraction pattern of tailing from Bangka mixed (below) and Sungkap (above).
Mnz – Monazite, Xtm – Xenotime, Qtz – Quartz, Ilm – Ilmenite, Cst – Cassiterite, Zrn – Zircon

Rys. 3. Wyniki dyfrakcji zmieszanych odpadów przeróbczych z Wyspy Bangka (poniżej) i Wyspy Sungkap (powyżej). Mzn – monacyt, Xtm – ksenotym, Qtz – kwarc, Ilm – ilmenit, Cst – kasyteryt, Zrn – cyrkon

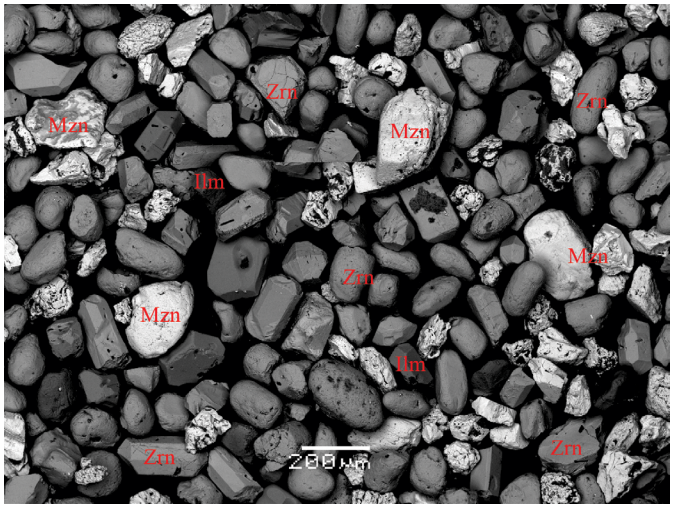

Fig. 4. Tailing from Toboali, sample 7BT.
Mnz – monazite; Zrn – zircon; Ilm – ilmenite. SEM-BSE image

Rys. 4. Odpad przeróbczy z Toboali, próbka 7BT.
Mnz – monacyt, Zrn – cyrkon, Ilm – ilmenit. Obraz SEM-BSE

Table 2. The content of minerals in concentrates calculated according to the Rietveld method in %

Tabela 2. Zawartość minerałów w koncentratach, wyliczona na podstawie metody Rietveld's w %

Sample / Mineral	5BT	6BB	7BT	10BB	21BP	22BS	23BL	25BP	27BK	32BM
Zircon	14.71	5.38	25.43	5.23	0.00	16.82	12.53	84.43	4.99	0.68
Xenotime	1.99	4.38	3.20	0.45	1.07	17.20	4.35	0.92	0.28	4.77
Monazite	2.02	4.71	1.96	1.56	90.60	21.00	5.33	11.15	0.82	–
Rutile	5.25	2.70	4.57	2.40	1.95	3.77	6.02	–	2.78	0.85
Anatase	2.81	1.54	0.77	0.30	–	0.92	1.46	–	0.30	–
Pseudorutile	48.02	24.61	25.29	4.32	–	7.80	29.48	–	4.67	36.70
Ilmenite	16.20	5.26	10.77	3.68	–	18.80	7.34	–	3.47	53.40
Cassiterite	0.78	2.18	3.18	6.04	6.18	8.50	1.48	1.30	1.04	3.60
Quartz	5.60	40.28	21.01	58.02	–	–	15.55	–	57.96	–
Tourmaline	–	6.18	2.80	18.00	–	–	4.10	–	2.48	–
Other*	2.62	2.78	1.00	–	0.20	5.19	15.04	2.20	21.11	–

* – Struverite, malayaite, marcasite, pyrite, plagioclase, topaz, aeschynite-(Y).

3.2. Ce-Monazite

The highest amounts of REE minerals are found in samples from Toboala (7BT), Sungkap (22BS), Pemali-Sungailiat (21BP and 25BP) and Lubuk (23BL) regions. The average monazite content is 3.51% (calculated on the 19 samples), which is 3 times higher (~1.1%) than in concentrates of heavy minerals produced in Australia (Mudd and Jowitt 2016).

The monazite amount in tailing varies from 0.82 to 90.60%. Monazite forms crystals of euhedral, subhedral and dominating in mass anhedral forms with sizes from 100 to 250 µm. Monazite is characterized by a medium to good degree of roundness with numerous internal cracks. Very often it forms intergrowths with xenotime. The observation of monazite grains (SEM-BSE) reveals the presence of porous zones resembling channels within which small new mineral phases such as: huttonite, thorite and uranothorite are crystallized (Fig. 4). These forms are characteristic of metasomatic process associated with the processes of dissolution and crystallization as a result of interaction of grains with hydrothermal fluids (Hetherington and Harlov 2008; Hetherington et al. 2010). Crystallization of the intergrowths in the monazite probably results from lower Th solubility in relation to REE in hydrothermal fluids (Hetherington et al. 2010). U-Th minerals form small structures from a few to several µm (Fig. 5). The iso-structural substitution of thorium and uranium (as elements) takes place in

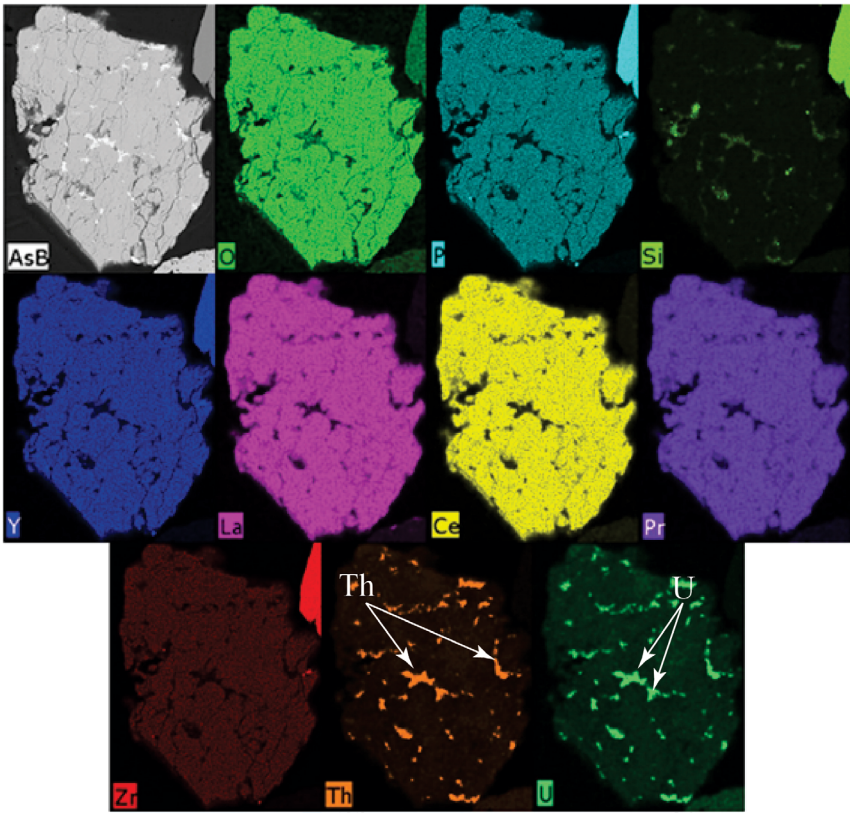

Fig. 5. Selected elements (P, Si, Y, La, Ce, Pr, Zr) in monazite grain as well as Th-U inclusions. SEM-BSE images

Rys. 5. Wybrane pierwiastki (P, Si, Y, La, Ce, Pr, Zr) w monacycie, wraz z inkluzjami Th-U. Obrazy SEM-BSE

the monazite, forming inclusions of up to 4-5 µm. Monazites demonstrate characteristic zoning related to Si, Th, Y and U varying content (Zhu and O'Nions 1999; Gibson et al. 2004).

On the basis of SEM-BSE photos (Fig. 6A–D) and WDS spectra analyses, three types of internal textures of monazites were distinguished:

- complex "intergrowth-like" zoning (Fig. 6A);
- oscillatory zoning (Fig. 6B);
- patches with numerous Th-U phases intergrowths in porous space (Fig. 6C–D).

Monazite belongs to the group of minerals of the cerium type, which builds LREE into its structure. A single monoclinic crystal structure can absorb REE with larger diameters (1.18–1.07 Å) due to the fact that the coordination number of the REO polyhedron in the monazite is 9 (Ni et al. 1995; Clavier et al. 2011). HREEs, which are smaller (1.07–0.97 Å) and usually have a lower coordination number (Ni et al. 1995; Kanazawa and Kamitani 2006).

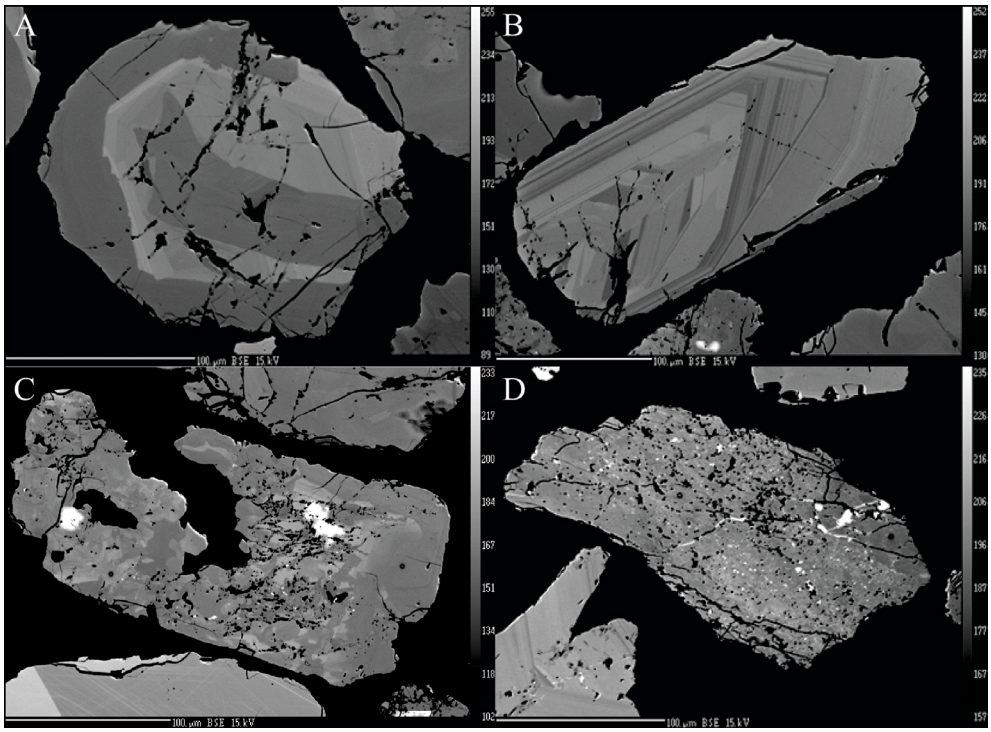

Fig. 6. (A) "intergrowth-like" complex zoning structure; (B) oscillatory zoning structure; (C–D) patchy structure with many inclusions Th-U phases. SEM-BSE image

Rys. 6. (A) strefowa struktura wrostkowa; (B) oscylacyjna struktura strefowa; (C–D) struktura patchworkowa z wieloma drobnymi inkluzjami faz Th-U. Obraz SEM-BSE

Micro-area analyses of monazite grains (Table 3) revealed maximal content of P_2O_5 up to 29.27 wt.%, and up to 33.50 wt.% of Ce_2O_3. Increased concentrations form La_2O_3 up to 15.46 wt.% and Nd_2O_3 up to 12.87 wt.%. SiO_2, CaO and PbO are present in trace amounts. Total REE_2O_3+Y content in monazites ranges from 58.18 to 65.90 wt.% (average 62.80), while LREO content ranges from 56.55 to 63.32 wt.% and HREO from 1.62 wt.% to 4.79 wt.%. Monazites are characterized by a high ThO_2 content (up to 11.30 wt.%), in contrast to a low amount of UO_2 (up to 0.35 wt.%). The Th/U ratio is very high and amounts up to 59.20. The content of radioactive elements in the monazite is at the level typical for magma environment (about 6.5 wt.%) and is significantly lower than for pegmatite monazites (Mannucci et al. 1986).

All grains are characterized by a high content of the X_{mnz} monazite molecule from 0.839 to 0.963. There is a process of thorium substitution in minerals and to a lesser extent uranium substitution in the crystallographic grid towards huttonite/thorite (Fig. 7). The normalization diagram (Fig. 8) with respect to chondrite C1 (McDonough and Sun 1995) indicates the enrichment of LREE with respect to HREE. There is a constant decrease from La to Sm,

$(La/Nd)_n$ from 1.768 to 3.361. Using EPM, a strong Eu anomaly was detected, where Eu/Eu* $[Eu_n/(Sm_n \cdot Gd_n)]^{1/2}$ is up to 0.138. The cerium anomaly Ce/Ce* $[Ce_n/(La_n \cdot Pr_n)]^{1/2}$ is from 1.112 to 1.239.

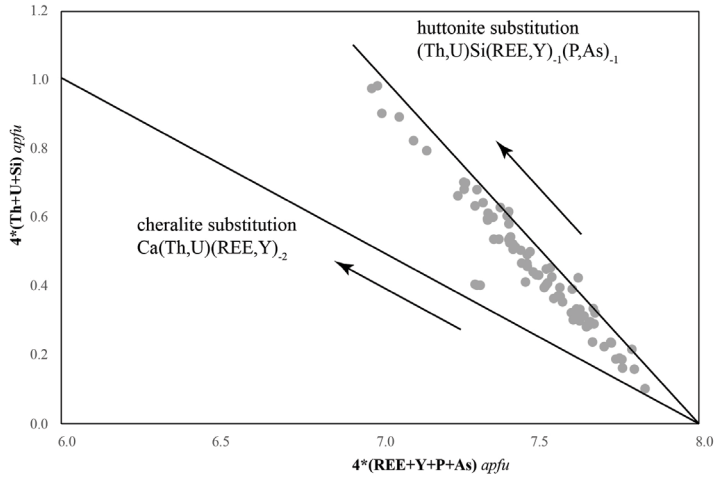

Fig. 7. The plot substitution diagram: Th+U+Si vs. REE+Y+(P+As) in monazite to huttonite (Th,U)Si(REE,Y)-1 (P,As)-1 with the ideal huttonite/thorite substitution vectors (straight lines)

Rys. 7. Diagram podstawień: Th+U+Si vs. REE+Y+(P+As) w monacycie do huttonitu (Th,U)Si(REE,Y)-1 (P,As)-1 z idealnymi huttonit/toryt zastępowaniami wektorowymi (proste linie)

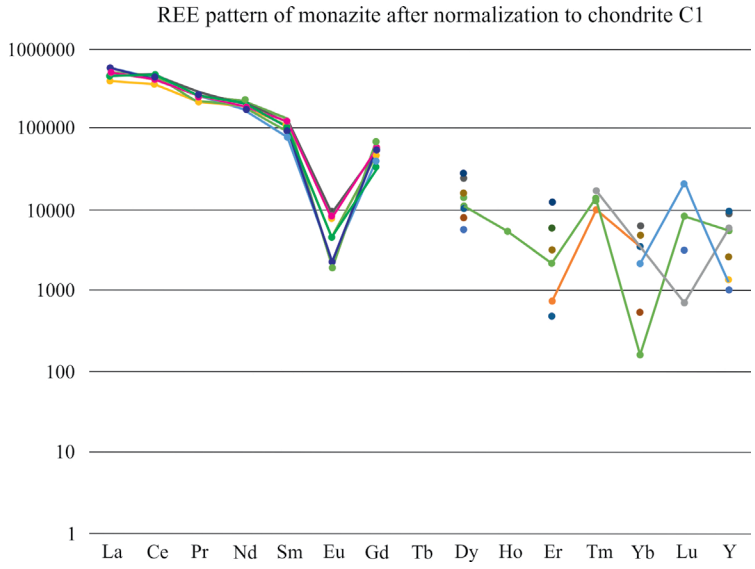

Fig. 8. Normalized chondrite-C1diagram of REE pattern in monazite grains

Rys. 8. Diagram znormalizowanego chondrytu-C1 z REE w monacycie

Table 3. Chemical compositions of monazites. [wt.%]

Tabela 3. Skład chemiczny monacytów. [% wag.]

Sample wt.%	1	2	3	4	5	6	7	8	9	10	11	12	13	14	15	16
SiO_2	0.95	1.31	0.96	0.43	0.42	1.75	0.96	2.89	1.62	0.91	0.78	0.97	0.75	0.93	0.65	1.82
P_2O_5	28.28	27.85	28.20	29.08	29.06	26.83	28.20	26.37	28.41	29.27	29.17	28.84	28.54	29.32	30.01	28.07
CaO	0.23	0.16	0.12	1.77	1.739	0.12	0.12	0.06	0.17	0.26	0.19	0.14	0.82	0.08	0.31	0.19
La_2O_3	13.22	15.03	15.36	11.83	11.86	15.46	15.36	14.60	13.52	12.63	13.32	13.91	13.18	15.15	13.78	12.75
Ce_2O_3	32.02	31.54	33.50	27.12	27.45	31.15	33.50	28.53	29.00	30.87	30.20	30.53	29.20	33.62	30.62	27.88
Pr_2O_3	3.29	2.73	2.97	2.94	2.91	2.53	2.97	2.46	2.60	2.88	2.80	2.88	2.92	2.92	2.76	2.72
Nd_2O_3	11.82	9.57	10.01	12.37	12.87	8.82	10.01	9.69	10.99	12.84	12.19	12.22	10.89	11.38	12.94	11.92
Sm_2O_3	2.18	1.60	1.45	2.22	2.09	1.34	1.45	1.37	2.01	2.65	2.35	2.42	1.90	1.69	2.64	2.44
Eu_2O_3	0.03	0.05	0.01	1.25	0.01	0.05	0.01	bdl	bdl	bdl	bdl	bdl	bdl	bdl	bdl	bdl
Gd_2O_3	1.29	0.96	0.91	bdl	1.26	0.94	0.91	0.78	1.24	1.12	1.57	1.63	1.18	0.84	1.78	1.41
Tb_2O_3	bdl	bdl	bdl	0.09	bdl	bdl	bdl	bdl	bdl	bdl	bdl	bdl	bdl	bdl	bdl	bdl
Dy_2O_3	0.29	0.30	0.29	bdl	0.16	0.31	0.29	0.23	0.72	0.46	0.81	0.41	0.48	0.17	0.17	0.46
Ho_2O_3	bdl	bdl	bdl	bdl	bdl	0.03	bdl	bdl	bdl	bdl	bdl	bdl	bdl	bdl	bdl	bdl
Er_2O_3	bdl	0.01	bdl	bdl	bdl	0.04	bdl	0.04	bdl	0.06	0.23	0.11	bdl	0.03	bdl	0.10
Tm_2O_3	bdl	0.02	0.04	bdl	0.03	0.04	bdl	bdl	bdl	bdl	bdl	bdl	bdl	bdl	bdl	bdl
Yb_2O_3	0.04	0.06	0.06	bdl	bdl	bdl	0.06	0.01	0.12	0.09	bdl	bdl	bdl	bdl	bdl	0.02
Lu_2O_3	0.06	bdl	bdl	bdl	0.09	0.02	bdl	bdl	bdl	bdl	bdl	bdl	bdl	bdl	bdl	bdl
Y_2O_3	0.25	1.13	1.23	0.27	0.20	1.07	1.23	0.93	1.84	0.52	2.18	0.88	1.76	0.20	0.42	1.41
ThO_2	4.80	5.57	4.53	8.98	8.93	7.71	4.53	11.30	6.93	4.84	2.82	4.26	7.87	3.93	3.68	8.20
UO_2	0.08	0.24	0.10	0.28	0.32	0.23	0.10	0.33	0.24	0.14	0.35	0.15	0.19	0.11	0.15	0.18

Table 3. cont.

Tabela 3. cd.

Sample wt.%	1	2	3	4	5	6	7	8	9	10	11	12	13	14	15	16
PbO	0.02	0.04	bdl	0.20	0.19	0.05	bdl	0.07	0.04	0.02	0.04	bdl	0.06	bdl	0.01	bdl
Total	**98.92**	**98.25**	**99.83**	**98.94**	**99.59**	**98.57**	**99.77**	**99.56**	**99.45**	**99.66**	**99.00**	**99.35**	**99.74**	**100.37**	**99.92**	**99.57**
$\Sigma REE_2O_3+Y_2O_3$	64.53	63.05	65.90	58.18	58.90	61.85	65.85	58.54	62.04	64.22	65.65	64.99	61.51	66.00	65.11	61.11
ΣLREO	62.59	60.54	63.32	56.56	57.22	59.37	63.32	56.55	58.12	61.87	60.86	61.96	58.09	64.76	62.74	57.71
$\Sigma HREO+Y_2O_3$	1.94	2.51	2.57	1.62	1.67	2.48	2.52	1.99	3.92	2.35	4.79	3.03	3.42	1.24	2.37	3.40
Apfu based on 4 oxygens																
Si	0.038	0.053	0.038	0.017	0.034	0.072	0.038	0.117	0.064	0.036	0.031	0.039	0.030	0.036	0.025	0.072
P	0.963	0.952	0.954	0.981	0.978	0.926	0.954	0.901	0.952	0.978	0.976	0.970	0.962	0.974	0.992	0.944
Ca	0.010	0.007	0.005	0.076	0.074	0.005	0.005	0.003	0.007	0.011	0.008	0.006	0.035	0.003	0.013	0.008
La	0.196	0.224	0.226	0.174	0.174	0.233	0.226	0.217	0.197	0.184	0.194	0.204	0.194	0.219	0.198	0.187
Ce	0.471	0.466	0.490	0.396	0.400	0.465	0.490	0.421	0.420	0.446	0.437	0.444	0.426	0.483	0.438	0.406
Pr	0.048	0.040	0.043	0.043	0.042	0.038	0.043	0.036	0.037	0.041	0.040	0.042	0.042	0.042	0.039	0.039
Nd	0.170	0.138	0.143	0.176	0.183	0.128	0.143	0.138	0.155	0.181	0.172	0.173	0.155	0.160	0.180	0.169
Sm	0.030	0.022	0.020	0.031	0.029	0.019	0.020	0.019	0.027	0.036	0.032	0.033	0.026	0.023	0.036	0.033
Eu	0.000	0.001	0.000	0.001	0.000	0.001	0.000	0.000	0.000	0.000	0.000	0.000	0.000	0.000	0.000	0.000
Gd	0.017	0.013	0.012	0.017	0.017	0.013	0.012	0.010	0.016	0.016	0.021	0.021	0.016	0.011	0.023	0.019
Tb	0.000	0.000	0.000	0.000	0.000	0.000	0.000	0.000	0.000	0.000	0.000	0.000	0.000	0.000	0.000	0.000
Dy	0.004	0.004	0.004	0.001	0.002	0.004	0.004	0.003	0.009	0.006	0.010	0.005	0.006	0.002	0.002	0.006
Ho	0.000	0.000	0.000	0.000	0.000	0.000	0.000	0.000	0.000	0.000	0.000	0.000	0.000	0.000	0.000	0.000
Er	0.000	0.000	0.000	0.000	0.000	0.001	0.000	0.001	0.000	0.001	0.003	0.001	0.000	0.000	0.000	0.001

Table 3. cont.

Tabela 3. cd.

Sample wt.%	1	2	3	4	5	6	7	8	9	10	11	12	13	14	15	16
Tm	0.000	0.000	0.001	0.000	0.000	0.001	0.000	0.000	0.000	0.000	0.000	0.000	0.000	0.000	0.000	0.000
Yb	0.000	0.001	0.001	0.000	0.000	0.000	0.001	0.000	0.001	0.001	0.000	0.000	0.000	0.000	0.000	0.000
Lu	0.001	0.000	0.000	0.000	0.000	0.000	0.000	0.000	0.000	0.000	0.000	0.000	0.000	0.000	0.000	0.000
Y	0.005	0.024	0.026	0.006	0.004	0.023	0.026	0.020	0.039	0.011	0.046	0.019	0.037	0.004	0.009	0,030
Th	0.044	0.051	0.041	0.081	0.081	0.072	0.041	0.104	0.062	0.043	0.025	0.038	0.071	0.035	0.033	0.074
U	0.001	0.002	0.001	0.002	0.003	0.002	0.001	0.003	0.002	0.001	0.003	0.001	0.002	0.001	0.001	0.002
Pb	0.000	0.000	0.000	0.002	0.002	0.001	0.000	0.001	0.000	0.000	0.000	0.000	0.001	0.000	0,000	0.000
Total	**2.000**	**1.999**	**2.006**	**2.005**	**2.006**	**2.002**	**2.006**	**1.993**	**1.992**	**1.992**	**1.999**	**1.996**	**2.003**	**1.994**	**1.990**	**1.991**
Molecular fraction																
X_{MNZ}	0.945	0.939	0.953	0.839	0.842	0.921	0.953	0.887	0.926	0.943	0.963	0.954	0.893	0.960	0.952	0.914
X_{CHER}	0.020	0.014	0.010	0.151	0.147	0.011	0.010	0.005	0.015	0.022	0.016	0.012	0.069	0.007	0.027	0.017
X_{HUT}	0.035	0.047	0.037	0.010	0.012	0.069	0.037	0.107	0.059	0.035	0.021	0.034	0.038	0.033	0.022	0.069
X_{LREE}	0.916	0.891	0.923	0.820	0.828	0.883	0.923	0.014	0.838	0.888	0.876	0.896	0.843	0.926	0.891	0.834
X_{HREE}	0.022	0.018	0.018	0.018	0.019	0.019	0.017	0.832	0.027	0.024	0.034	0.028	0.022	0.013	0.025	0.026
Th/U	59.21	23.76	43.79	32.69	27.953	33.0	43.79	35.02	29.53	35.36	8.24	29.04	42.81	36.52	25.09	46.59
Normalized to chondrite C1																
Ce/Ce*	1.175	1.192	1.201	1.112	1.130	1.205	1.201	1.153	1.184	1.239	1.197	1.168	1.140	1.224	1.202	1.146
Eu/Eu*	0.056	0.125	0.039	0.111	0.028	0.138	0.039	0.000	0.000	0.000	0.000	0.000	0.000	0.000	0.000	0.000
La/Nd_n	2.145	3.010	2.940	1.834	1.768	3.361	2.940	2.920	2.359	1.886	2.096	2.183	2.321	2.553	2.042	2.051

From the chemical point of view (Table 3) monazites originate from magma rocks. Compared to loose monazites found in placer deposits of Western Australia (Jaireth et al. 2014; Van Emden et al. 1997), analyzed monazites are enriched in Ce_2O_3 (up to 29.63%), Nd_2O_3 (up to 11.08%), Y_2O_3 (up to 1.67%), Gd_2O_3 (up to 1.32%) and UO_2 (up to 0.32%).

3.3. Source of monazite grains

Granites from Bangka Island were classified as syn-collision and WPG granites (Wai-Pan Ng et al. 2017). According to Pearce (Pearce et al. 1984), rocks formed under these tectonic conditions are characterized by increased REE and Y concentrations. Granites of Indonesian islands: Bangka (Wai-Pan Ng et al. 2017), Singkep (Ikuno et al. 2010) and Belitung (Soetopo et al. 2012) as well as Main Range granite province SW of Thailand and western Malaysia are characterized by the presence of tin-tantalum-REE mineralization

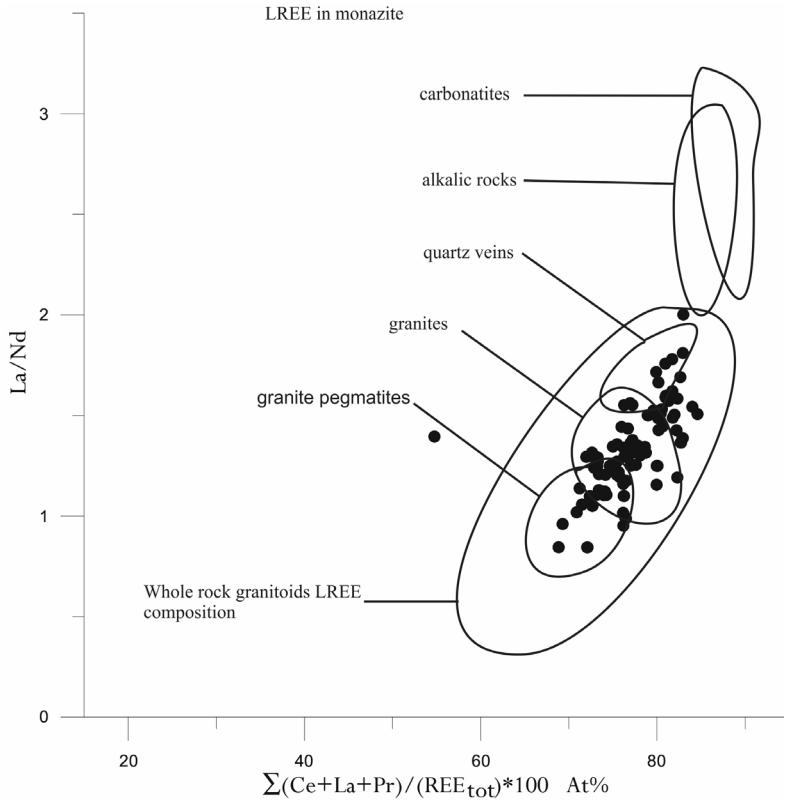

Fig. 9. Source rocks for monazite grains inferred from LREE distribution in analyzed crystals (Rapp and Watson 1986)

Rys. 9. Skała macierzysta dla monacytu określona na podstawie dystrybucji LREE w analizowanych kryształach

zone (Searle et al. 2012). Granites from Bangka Island (Wai-Pan Ng et al. 2017) reveal anomalously high content of REE (Nama granite up to 1045.1 ppm ΣREE). The main carriers of REE are monazite and xenotime, which are an accessory fraction of granite massifs (Schwartz et al. 1995). Intensive processes of chemical weathering from the Neogene to the present day of granite structures led to the formation of Quaternary colluvial, alluvial and coastal placers enriched with heavy minerals (Schwartz et al. 1995). According to Aryanto and Kamiludin (2016), anomalous monazite contents of up to 67.8 g/m^3 were recorded in the southern part of Bangka Island, in sand sediments from the Toboala region.

The phase composition of the tailing from Bangka Island proves that the sources of minerals accompanying the placer sediments tin mineralization are granitoids (Fig. 9). In tailing there is a lack of diagnostic minerals for metamorphic and mafic magma rocks. A high concentration of ilmenite, lack of magnetite, low ratio of HREE to YPO_4 in xenotimes, proves that the source of minerals of REE carriers are granitoides of ilmenite series S.

The ratio of ThO_2 to UO_2 and negative cerium anomaly (Zhu and O'Nions 1999) in monazites indicate that their sources of grains are granitoides or pegmatite granitoides (Fig. 10). The results of several analyses show that the monazite was also formed under hydrothermal conditions (Janots et al. 2012).

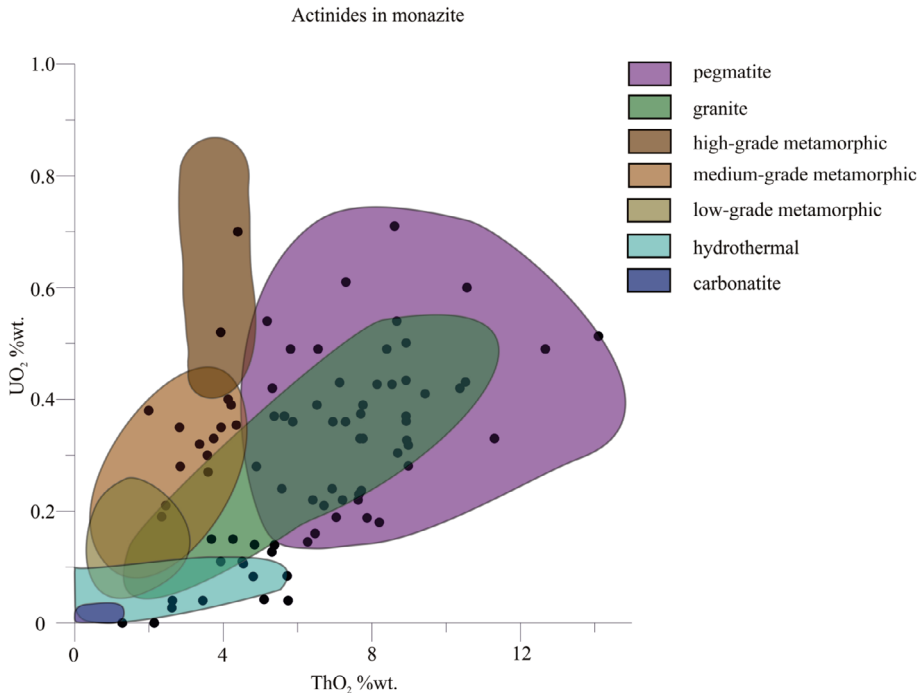

Fig. 10. Th and U concentration data of the studied monazite (black dots) compared with selected literature (Janots et al. 2012, modified)

Rys. 10. Koncentracja U i Th w badanych monacytach (czarne kropki) w porównaniu z danymi z wybranej literatury

3.4. The potential of monazite resources on Bangka Island

Indonesia's Center of Geological Resources (Harjanto et al. 2013) estimates that the reserves of rare earth minerals and zircon in the tin mining areas amount to 951.000 t. The average monazite content in the tin bearing sand deposits is 0.67–1.31% (Rapp and Watson 1986). The hypothetical monazite resources on the coast of Bangka Island have been estimated at 471,087,689 m^3 (Aryanto and Kamiludin 2016). Due to lack of public information on tailing production by state companies and very large territorial dispersion of the compradors, as indicated by (Szamałek et al. 2013), it is difficult to determine the actual production capacity of monazite concentrates. The analysis of the production path of state-owned smelters may make it possible to estimate the resources and production capacity of monazite concentrates. The processing of cassiterite sands in the state smelters allow to obtain concentrates: zircon ≥85%, ilmenite ≥ 80%, monazite ≥ 60% and slags (Handoko and Sanjaya 2018; Harjanto et al. 2013).

Tailing from Bangka Island has a high resource potential. The efficiency of the heavy mineral separation process indicates the yield of the final polymineral concentrate with a considerable content of cassiterite, Ti oxides, monazite, xenotime, zircon and other mineral phases of deposit importance. The introduction of "circular economy" principles may allow to increase the processing and recovery efficiency of valuable mineral phases, which are now irretrievably lost.

An estimation of the possible real annual production of monazite concentrate has been made, with the result of 7000 t. It indicates that Bangka Island could become one of the main producers of TREO. Currently (Gambogi 2016) the world produces 9430 tons of monazite concentrate, and the main producers are: Brazil (3,700 tons), Thailand (2,600 tons) and India (2,500 tons).

3.5. Industrial minerals

Natural and synthetic monazites are used mainly as: diffusion coatings and barriers, for geochronological dating, as phosphors, lasers and light emitters, as ionic conductors and as matrices for the storage of radioactive materials (Clavier et al. 2011; Handoko and Sanjaya 2018; Förster 1998). Monazite is one of the few minerals currently used as a source of rare earth elements (Kanazawa and Kamitani 2006; Simandl 2014; Golev et al. 2014; Elsner 2013). Tailing and monazites presented in it are characterized by a high Th content. It limits the possibility of mono-element REE concentrates production. Initial radioactivity studies of monazite-rich tailing (21BP sample) indicate that ^{232}Th activity is $A_{Th} = 340 \pm 10$ Bq. It means that the Th content in the 8.3 g sample is at the level of $m_{Th} = 83 \pm 8$ mg, which is 1% of the sample mass. Uranium activity is $^{238}U = 114 \pm 2$ Bq, which is 0.1% of the sample weight.

Worldwide reports show that it is difficult to make a mining project economically viable, where the extracted mineral resource is mainly composed of highly radioactive minerals.

The lowest cost of obtaining ThO_2 from monazite bearing sands occurs at a production level of 10 t ThO_2 (Mohd Salehuddin et al. 2019). The estimated cost of obtaining 1 t ThO_2 is $ 3540.95 $3592.94 kg^{-1} and for 10t ThO_2 $ 501.18–553.17 kg^{-1}. High costs are associated with REE separation, radioactive waste storage and land rehabilitation (Bahari 2007). This results in monazite usually being treated as waste and is disposed of, or stored (Golev et al. 2014). The increase in the raw material potential of the monazite depends closely on the development of nuclear power plants based on thorium (Simandl 2014; Ault et al. 2015).

Conclusion

Detailed studies of tailing obtained after processing of cassiterite bearing sediments revealed anomalous high monazite contents of up to 90.60 wt.% and the presence of other minerals of REE bearers (xenotime, unidentified phases of REE-Nb-Y-Ti). The studied monazite belongs to the group of monazites of the cerium type. Monazite grains are characterized by numerous internal cracks filled with small mineral phases containing of Th and U. Chemical analyses of monazite in the micro-area showed the content of grains up to 33.50 wt.% of Ce_2O_3 and increased La_2O_3 content to 15.46 wt.% and Nd_2O_3 to 12.87 wt.%. The average total REE_2O_3 + Y content in monazites is 62.80 wt.%. The monazites chemical composition is typical for the minerals originating from magma.

The mineral composition of the examined tailing indicates its high resource potential of industrial minerals. The three-stage pre-treatment of tin bearing sediments by local compradors has a low efficiency of the enrichment process. However, the resulting waste (quantitatively and qualitatively) is a valuable mineral raw material for further technologically advanced processing. The extraction of mineral raw materials from secondary sources (anthropogenic accumulations) allows for balancing the demand with the supply. Moreover, the exploitation of anthropogenic accumulations reduces the need to increase the extraction of mineral raw materials from primary sources (mineral deposits), which is beneficial for the natural environment. Such an action is consistent with the principles of "circular economy" reducing the waste stream, increasing the effectiveness of raw material management and processing. The utilization of monazite bearing waste in the Indonesian Islands can be an important factor for development and economic activation. Studies have shown that mining waste on Bangka Island can be a valuable resource reserve for REE subject to separation and ensuring the economic use of thorium. The presence of radioactive elements at the moment is a crucial technological obstacle in processing in use of such raw materials.

The article has been prepared in the framework of the statutory research performed in the PGI-NRI, titled „Mineralogia odpadów po przeróbce osadów kasyterytonośnych – Wyspa Bangka, Indonezja" – No. 62.9012.1967.00.0.

REFERENCES

Aleva, G.J.J. 1960. The plutonic igneous rocks from Billiton. Indonesia. *Geol. Mijnbouw* 39, pp. 427–436.

Aryanto, N.C.D. and Kamiludin, U. 2016. The Content of Placer Heavy Mineral and Characteristics of REE at Toboali Coast and Its Surrounding Area. Bangka Belitung Province. *Bulletin of the Marine Geology* 31(1), pp. 45–54.

Ault et al. 2015 – Ault,T., Krahn, S. and Croff, A. 2015. Assessment of the Potential of By-Product Recovery of Thorium to Satisfy Demands of a Future Thorium Fuel Cycle. *Nucl. Technol*. 189(2), pp. 152–162.

Bahari et al. 2007 – Bahari, I., Mohsen, N. and Abdullah, P. 2007. Radioactivity and radiological risk associated with effluent sediment containing technologically enhanced naturally occurring radioactive materials in amang (tin tailings) processing industry. *J. Environ. Radioact*. 95, pp. 161–170.

Clavier et al. 2011 – Clavier, N., Podor, R. and Dacheux, N. 2011. Crystal chemistry of the monazite structure. *J. Eur. Ceram. Soc*. 31, pp. 941–976.

Cobbing et al. 1992 – Cobbing, E.J., Pitfield, P.E.J., Darbyshire, D.P.F. and Mallick, D.I.J. 1992. The Granites of the South-East Asian Tin Belt. British Geological Survey, London.

Deady et al. 2014 – Deady, E., Mouchos, E., Goodenough, K., Williamson, B. and Wall, F. 2014. Rare Earth Elements in Karst-Bauxites: a Novel Untapped European Resource? *ERES2014 1st Eur. Rare Earth Resour. Conf., Milos, Greece,* 4–7 Sept. 2014.

Elsner, H. 2013. *Heavy Minerals of Economic Importance*. BGR: Hannover. Germany, pp. 1–218.

European Commission. List of Critical Raw Materials for the EU. 2017. *Commun. from Comm. to Eur. Parliam. Counc. Eur. Econ. Soc. Comm. Comm. Reg.*

Förster, H.J. 1998. The chemical composition of REE-Y-Th-U-rich accessory minerals in peraluminous granites of the Erzgebirge-Fichtelgebirge region. Germany. Part I: The monazite-(Ce)-brabantite solid solution series. *Am. Mineral*. 83(3–4), pp. 259–272.

Gambogi, J. 2016. *USGS 2016 Minerals Yearbook Thorium [Advance Release]*. Publisher: USGS, Reston, Virginia, US, pp 77.1–77.5.

Gibson et al. 2004 – Gibson, H.D., Carr, S.D., Brown, R.L. and Hamilton, M.A. 2004. Correlations between chemical and age domains in monazite. and metamorphic reactions involving major pelitic phases: an integration of ID-TIMS and SHRIMP geochronology with Y-Th-U X-ray mapping. *Chem. Geol*. 211, pp. 237–260.

Golev et al. 2014 – Golev, A., Scott, M., Erskine, P.D., Ali, S.H. and Ballantyne, G.R. 2014. Rare earths supply chains: Current status, constraints and opportunities. *Resour. Policy* 41, pp. 52–59.

Goodenough et al. 2018 – Goodenough, K. M., Wall, F. and Merriman, D. 2018. The Rare Earth Elements: Demand, Global Resources, and Challenges for Resourcing Future Generations. *Nat. Resour. Res.* 27, pp. 201–216.

Haldar, S.K. 2013. *Mineral exploration principles and applications*. Elsevier: Waltham, USA, pp. 55–71.

Handoko, A.D. and Sanjaya, E. 2018. Characteristics and genesis of Rare Earth Element (REE) in western Indonesia. In *IOP Conference Series: Earth and Environmental Science*.

Harjanto et al. 2013 – Harjanto, S., Virdhian, S. and Afrilinda, E. 2013. Characterization of Indonesia rare earth minerals and their potential processing techniques. Proceedings of the Conference: Rare Earth Elements. October.

Hetherington. C.J. and Harlov. D.E. 2008. Metasomatic thorite and uraninite inclusions in xenotime and monazite from granitic pegmatites. Hidra anorthosite massif. southwestern Norway: Mechanics and fluid chemistry. *Am. Mineral*. 93, pp. 806–820.

Hetherington et al. 2010 – Hetherington, C.J., Harlov, D.E. and Budzyń, B. 2010. Experimental metasomatism of monazite and xenotime: mineral stability. REE mobility and fluid composition. *Miner. Petrol*. 99, pp. 165–184.

Hoatson et al. 2011 – Hoatson, D.M., Jaireth, S. and Miezitis, Y. 2011. *The major rare-earth-element deposits of Australia: geological setting, exploration, and resources*. Geoscience Australia, 204 pp.

Hutchison, C.S. and Taylor, D. 1978. Metallogenesis in SE Asia. *J. Geol. Soc. London.* 135, pp. 405–428.

Ikuno T. et al. 2010. Concentration and Geochemical behavior of REE in Hydrothermally Altered and Weathered Granitic Rocks in Southern Thailand and Bangka Island, Indonesia Int. Symposium on Earth Science and Technology, pp. 269–273.

Ishihara, S. 1977. The magnetite-series and ilmenite-series granitic rocks. *Mining Geol*. 27, pp. 293–305.

Jaireth et al. 2014 – Jaireth, S., Hoatson, D.M. and Miezitis, Y. 2014. Geological setting and resources of the major rare-earth-element deposits in Australia. *Ore Geol. Rev*. 62, pp. 72–128.

Janots et al. 2012 – Janots, E., Berger, A., Gnos, E. Whitehouse, M., Lewin, E. and Pettke, T. 2012. Constraints on fluid evolution during metamorphism from U-Th-Pb systematics in Alpine hydrothermal monazite. *Chem. Geol*. 326–327, pp. 61–71.

Kanazawa, Y. and Kamitani, M. 2006. Rare earth minerals and resources in the world. *Journal of Alloys and Compounds*. 408–412, pp. 1339–1343.

Ko Ko, U. 1986. Preliminary synthesis of the geology of Bangka Island, Indonesia. *Bull. Geol. Soc. Malaysia* 20, pp. 81–96.

Mannucci et al. 1986 – Mannucci, G., Diella, V., Gramaccioli, G.M. and Pilati, T. 1986. A comparative study of some pegmatitic and fissure monazite from the Alps. *Can. Mineral*. 24, pp. 469–474.

McDonough, W.F. and Sun, S.S. 1995. The composition of the Earth. *Chem. Geol*. 67(5), pp. 1050–1056.

Metcalfe, I. 2002. Permian tectonic framework and palaeogeography of SE Asia. *J. Asian Earth Sci.* 20, pp. 551–556.

Mohd Salehuddin et al. 2019 – Mohd Salehuddin, A.H.J., Ismail, A.F., Che Zainul Bahri, C.N.A. and Aziman, E.S. 2019. Economic analysis of thorium extraction from monazite. *Nucl. Eng. Technol.* 51(2), pp. 631–640.

Mudd, G.M. and Jowitt, S.M. 2016. Rare earth elements from heavy mineral sands: assessing the potential of a forgotten resource. *Applied Earth Science*. 125(3), pp. 107–113.

Ni et al. 1995 – Ni, Y., Hughes. J.M. and Mariano, A.N. 1995. Crystal chemistry of the monazite and xenotime structures. *Am. Mineral*. 80, pp. 21–26.

Pearce et al. 1984 – Pearce, J.A., Harris, N.B.W. and Tindle, A.G. 1984. Trace element discrimination diagrams for the tectonic interpretation of granitic rocks. *J. Petrol.* 25, pp. 956–983.

Periravi et al. 2017 – Periravi, M., Ackah, L., Guru, R., Mohanty, M. and Liu, J. 2017. Chemical extraction of rare earth elements from coal ash. *Miner. Metall. Process.* pp. 17–128.

Priem et al. 1975 – Priem, H.N.A., Boelrijk, N.A.I.M., Bon, E.H., Hebeda, E.H., Verdurmen, E.A.T. and Verschure, R.H. 1975. Isotope Geochronology in the Indonesian Tin Belt. *Geol. Mijnbouw.* 54, pp. 61–70.

Rapp, R.P. and Watson, E.B. 1986. Monazite solubility and dissolution kinetics: implications for the thorium and light rare earth chemistry of felsic magmas. *Contrib. Mineral. Petrol*. 94, pp. 304–316.

Schwartz et al. 1995 – Schwartz, M.O., Rajah, S.S., Askury, S.K., Putthapiban, P. and Djaswadi, S. 1995. The Southeast Asian tin belt. *Earth-Sci. Rev.* 38, pp. 95–293.

Schwartz, M.O. and Surjono. 1991. The Pemali tin deposit, Bangka, Indonesia. *Miner. Depos.* 26, pp. 18–25.

Searle et al. 2012 – Searle, M.P., Whitehouse, M.J., Robb, L.J., Ghani, A.A., Hutchison, C.S., Sone, M., Wai-Pan Ng, S., Roselee, M.H., Chung, S.-L. and Oliver, G.J.H. 2012. Tectonic evolution of the Sibumasu-Indochina terrane collision zone in Thailand and Malaysia: constraints from new U-Pb zircon chronology of SE Asian tin granitoids. *J. Geol. Soc. London.* 169, pp. 489–500.

Simandl, G.J. 2014. Geology and market-dependent significance of rare earth element resources. *Miner. Depos.* 49, pp. 889–904.

Soetopo et al. 2012 – Soetopo, B., Subiantoro, L., Sularto, P. and dan Haryanto, D. 2012. The study of monazite and zircon in quarternary rocks in cerucuk belitung. (Studi Deposit Monasit dan Zirkon Dalam Batuan Kuarter di Daerah Cerucuk Belitung). [Location]. Indonesia.

Szamałek, K. and Galos, K. 2016. Metals in Spent Mobile Phones (SMP) – a new challenge for mineral resources management. *Gospodarka Surowcami Mineralnymi – Mineral Resources Management* 22(4), pp. 45–58.

Szamałek et al. 2013 – Szamałek, K., Konopka, G., Zglinicki, K. and Marciniak-Maliszewska, B. 2013. New potential source of rare earth elements. *Gospodarka Surowcami Mineralnymi – Mineral Resources Management* 29(4), pp. 59–76.

Van Emden et al. 1997 – Van Emden, B., Thornber, M.R., Graham, J. and Lincoln, F.J. 1997. The incorporation of actinides in monazite and xenotime from placer deposits in Western Australia. *Can. Mineral* 35, pp. 95–104.

Wai-Pan Ng et al. 2017 – Wai-Pan Ng, S., Whitehouse, M.J., Roselee, M.H., Teschner,C., Murtadha, S., Oliver, G.J.H., Ghani, A.A. and Chang, S. 2017. Late Triassic granites from Bangka, Indonesia: A continuation of the Main Range granite province of the South-East Asian Tin Belt, *J. Asian Earth Sci*. 138, pp. 548–561.

Wikarno et al. 1984 – Wikarno, U., Suyatna, D.A.D. and Sukardi, S. 1984. Granitoids of Sumatra and the Tin Islands. In Proceedings of: Geology of Tin Deposits in Asia and the Pacific. Selected Papers from the International Symposium on the Geology of Tin Deposits held in Nanning. Nanning, China, October 26–30, Hutchison C.S. eds., Springer. Berlin. Heidelberg.

Yasukawa et al. 2015 – Yasukawa, K., Nakamura, K., Fujinaga, K., Machida, S., Ohta, J., Takaya, Y. and Kato, Y. 2015. Rare-earth, major, and trace element geochemistry of deep-sea sediments in the Indian Ocean: Implications for the potential distribution of REY-rich mud in the Indian Ocean. *Geochem. J*. 49, pp. 621–635.

Zhou et al. 2017 – Zhou, B., Li, Z. and Chen, C. 2017. Global Potential of Rare Earth Resources and Rare Earth Demand from Clean Technologies. *Minerals* 7(11), pp. 1–14.

Zhu, X.K. and O'Nions, R.K. 1999. Monazite chemical composition: some implications for monazite geochronology. *Contrib. Mineral. Petrol.* 137, pp. 351–363.

MONAZITE-BEARING POST PROCESSING WASTES AND THEIR POTENTIAL ECONOMIC SIGNIFICANCE

Keywords

Bangka Island, tailing, monazite, REE, industrial minerals, processing of minerals

Abstract

During the geological prospecting works conducted in 2013 on Bangka Island (Indonesia), high monazite content was identified in the wastes produced during processing of cassiterite deposits. Monazite, among 250 known minerals containing REE, is one of the most important minerals as primary source of REE.The monazite content in this waste is up to 90.60%. The phase composition of the investigated tailing proves that the sources of minerals accompanying the placer sediments tin mineralization are granitoids. The tailing is composed of numerous ore minerals, including monazite, xenotime, zircon, cassiterite, malayaite, struverite, aeschynite-(Y), ilmenite, rutile, pseudorutile and anatase. Monazite grains belong to the group of cerium monazite. Its grains are characterized by high content of Ce_2O_3 27.12–33.50 wt.%, La_2O_3 up to 15.46 wt.%, Nd_2O_3 up to 12.87%. The total REE_2O_3 + Y content ranges from 58.18 to 65.90 wt.%. Monazite grains observations (SEM-BSE) revealed the presence of porous zones filled with fine phases of minerals with U and Th content. The radiation intensity of ^{232}Th is A_{Th} = 340 ± 10 Bq and $^{238}A_U$ = 114 ± 2 Bq. High content of monazite and other REE minerals indicates that tailing is a very rich, potential source of REEs, although the presence of radioactive elements at the moment is a technological obstacle in their processing and use. The utilization of monazite bearing waste in the Indonesian Islands can be an important factor for development and economic activation of this region and an example of the good practice of circular economy rules.

ODPADY MONACYTONOŚNE I ICH POTENCJALNE ZNACZENIE GOSPODARCZE

Słowa kluczowe

wyspa Bangka, odpady przeróbcze, monacyt, REE

Streszczenie

W trakcie geologicznych prac prospekcyjnych prowadzonych w 2013 roku na indonezyjskiej wyspie Bangka stwierdzono wysokie zawartości monacytu w odpadach powstałych po przeróbce osadów kasyterytonośnych. Monacyt jest jednym z najważniejszych pierwotnych źródeł REE wśród 250 znanych minerałów zawierających REE. Zawartość monacytu w badanym odpadzie wynosi do 90,60%. Skład fazowy badanych odpadów wskazuje, że źródłem minerałów towarzyszących w cynonośnych złożach okruchowych były granitoidy. W składzie odpadu przeróbczego, metodą XRD zidentyfikowano obecność licznych minerałów złożowych, wśród nich: monacyt, ksenotym, cyrkon, kasyteryt, malayait, strüveryt, aeschynit-(Y), ilmenit, rutyl, pseudorutyl i anataz. Badania składu chemicznego ziaren monacytu z użyciem EPMA ujawniły, że należy on do grupy monacytu cerowego. Jego ziarna cechują się wysoką zawartością Ce_2O_3 27,12–33,50% wt., La_2O_3 do 15,46% wt., Nd_2O_3 do 12,87%. Całkowita zawartość REE_2O_3 + Y mieści się w zakresie od 58,18 do 65,90% wt. Obserwacje ziaren monacytu (BSE) ujawniły w nich obecność stref porowatych wypełnionych drobnymi fazami minerałów z udziałem U oraz Th. Aktywność promieniotwórcza ^{232}Th wynosi ATh = 340 ± 10 Bq, a ^{238}U = 114 ± 2 Bq. Wysoka zawartość monacytu oraz innych minerałów nośników REE wskazuje, że odpad przeróbczy stanowi bardzo bogate, potencjalne źródło pierwiastków ziem rzadkich, choć zawartość pierwiastków promieniotwórczych stanowi obecnie przeszkodę technologiczną w ich przetwarzaniu i wykorzystaniu. Wykorzystanie monacytonośnych odpadów z wysp Indonezji może być ważnym czynnikiem rozwoju i aktywizacji gospodarczej tego regionu oraz przykładem dobrej praktyki stosowania zasad gospodarki o obiegu zamkniętym.